Dear Reviewer:

We sincerely thank you for your thorough and constructive review of our manuscript. We have carefully revised the manuscript in response to your suggestions. In the revised manuscript, we refined the procedure for determining the number of modes of DSDs and updated the corresponding description in the *Data set and method* section. Accordingly, we updated the results and the corresponding figures. Additional details on the fitting configuration are provided in Appendix A1. Furthermore, six representative cases are presented in Appendix A2 to illustrate how unimodal, bimodal, and trimodal DSD fits were selected.

Below, we provide a point-by-point reply, detailing the changes made and the corresponding locations in the revised manuscript.

Comments: *The authors attribute multimodal DSDs to collision-coalescence processes and state that "Triple-mode events consistently exhibit the broadest DSD and highest Nf of large droplets, consistent with their higher LWC." However, analysis of fog events reveals contradictory patterns. In F4, F1-1, and F10, fog DSDs begin as trimodal with low Dmax values and transition toward bimodal and unimodal distributions.*

Answer: In the revised manuscript, to avoid confusion arising from conceptual ambiguity, fog cases are no longer classified by the number of modes. Accordingly, Table 1 and Figure 1 have been revised to present statistics of physical variables and mean spectra for DSDs with different numbers of modes. In addition, in the revised manuscript, peak diameters are no longer identified. Instead, a turning-point identification method was employed in addition to the gamma and lognormal fits, to determine the turning diameter D_{turn}, as defined by the following:

"*For a DSD defined on discrete diameter bins, the change rate of number concentration was first computed as*

$$\Delta n_i(D) = \frac{n_i(D) - n_{i+1}(D)}{n_i(D)}, i = 1,2,\ldots,19 \qquad (11)$$

where D *is the droplet diameter,* $n(D)$ *is the number concentration for each bin. The sign of* $\Delta n_i(D)$ *characterized the local trend of the DSD: a positive value indicates decreasing concentration with increasing diameter, whereas a negative value indicates increasing concentration with increasing diameter. The turning diameter* D_{turn} *was identified as the diameter where the sign of* $\Delta n_i(D)$ *change from positive to negative, with the additional requirement that the number concentrations on its right side of are nonzero. In addition, if the number concentration in the first bin is the highest in the DSD, the* D_{turn} *of the first mode is assigned a value of 2 μm.*"

Meanwhile, for unimodal, bimodal, and trimodal gamma and lognormal fits, the first intersection between adjacent fitted components is defined as D_{turn}, indicating that the mode begins at the next bin. The specific implementation in the manuscript is as follows:

"*To determine the number of modes and mode separating positions, each fog DSD was sequentially*

fitted with unimodal (i=1), bimodal (i=2), and trimodal (i=3) gamma and lognormal distributions as show below:

For the gamma distribution:

$$n(D) = \sum_{i=1}^{3} n_i(D) = \sum_{i=1}^{3} N_{0,i} D^{\mu_i} e^{-\lambda_i D} \quad (12)$$

where D is the droplet diameter, $n(D)$ is the number concentration for each bin, N_0, μ and λ are the intercept, shape and slope parameters, respectively. For the lognormal distribution:

$$n(D) = \sum_{i=1}^{3} n_i(D) = \sum_{i=1}^{3} \frac{N_{0,i}}{2\pi^{1/2} D_i ln\sigma_{g,i}} exp\left(-\frac{(lnD_i - lnD_{g,i})^2}{2(ln\sigma_{g,i})^2}\right) \quad (13)$$

where D is the droplet diameter, $n(D)$ is the number concentration for each bin, N_0 is the total number concentration, D_g is the geometric mean diameter and σ_g is the geometric standard deviation. Details of the upper and lower bounds used in the fitting of Eq. (12) and Eq. (13) are provided in the Appendix A1.

For each DSD, unimodal, bimodal, and trimodal gamma and lognormal fits were performed, yielding the corresponding sets of fitting parameters as well as the individual modal components. A fit was retained only if adjacent modal components intersected (mode 1-2 for bimodal fits; mode 1-2 and mode 2-3 for trimodal fits). The turning diameter D_{turn} was identified as the diameter of the first intersection of two adjacent modes, indicating that the mode begins at the next bin. If the first size bin of the DSD had the highest number concentration, it was identified as D_{turn} of the first mode. A fit was accepted only if all identified D_{turn}s did not fall within the same or adjacent size bins. Finally, the Akaike Information Criterion (AIC) and the Bayesian Information Criterion (BIC) are used to evaluate the performance of the accepted fits."

Because the procedure for determining the number of modes and D_{turn} of DSDs was refined, the corresponding figures, tables were also revised. For example, Figure 7b has been updated and include more DSDs to illustrate their evolution over the fog life cycle. Related descriptions in the manuscript have also been revised. For example, in Lines 258-262 of the revised manuscript, the description of the evolution of DSD over the fog life cycle in Fog Case 1-1 has been updated as follows:

"*During fog formation and development, the DSD transitions among unimodal, bimodal, and trimodal. As the LWC approaches its maximum, N_f in the 5-20 μm range decreased, while those above 20 μm increased rapidly, suggesting a mass transfer from smaller to larger droplets as the DSD broadens toward larger droplets. During this stage, the DSD is predominantly bimodal. After 2006/12/25 10:00, as N_f and LWC gradually decrease, the DSD again alternates between bimodal and trimodal (Figure 5).*"

Comments: *This inconsistency may indicate an error in the mode-identification algorithm.*

Answer: Thank you for the suggestion. In the revised manuscript, a turning-point identification method was incorporated together with the gamma and lognormal fits to determine the number of

DSD modes and the turning diameter D_{turn}. Detailed descriptions are provided in the *Data Set and Methods* section (Line 139-196). We have also revised the description of gamma and lognormal parameter settings for mode identification in Appendix A1 to improve clarity and readability. For example:

"*To minimize subjective influence, relatively broad bounds of* D_g *were assigned to the parameters under different values of i. For unimodal distributions (i = 1),* D_g *were constrained to the range 2-50μm. In bimodal distributions (i = 2), two candidate mode diameter combinations were considered: (2, 11 μm) and (2, 21 μm). Accordingly, different lower and upper bounds were specified for* D_g*. For the 2 and 11 μm combination, the bounds were set to 2-10 and 5-20 μm; for the 2 and 21 μm combination, the bounds were 2-10 and 15-50 μm. In trimodal distributions (i = 3), the bounds for* D_g *were set to 2-50μm, 5-20μm, 15-50μm. The discrete representation of the lognormal distribution parameter* σ_g *is given by*

$$ln\sigma_g = \left(\frac{\sum n_i(lnD_i - lnD_g)^2}{\sum n_i - 1}\right)^{1/2} \quad (19)$$

in which $lnD_g = \frac{\sum n_i lnD_i}{\sum n_i}$*. In this study, the maximum calculated value of* σ_g *is approximately 2.34. Therefore, the range of* σ_g *was set to 0-2.5. In the meantime,* N_0 *was set to 0-2000 cm*$^{-3}$*."*

Comments: *Visual inspection of Figures 4-8 reveals that the distinctions among tri/bi/unimodal distributions do not align with the classifications provided. For example, in F1-1 (Fig 6b, pre-maximum LWC period), the green distribution—classified as triple-mode—appears indistinguishable from the purple, orange, and blue distributions, which are classified as bimodal despite exhibiting equal or greater numbers of peaks. In pre-LWC-max Fog 10 (Fig 7B), minimal differences exist between the orange and yellow DSDs, classified as trimodal and bimodal respectively. The yellow DSD exhibits a third mode at 40 μm that is more pronounced than features in the orange DSD. Before publication, the authors must verify that their algorithm identifies distribution types. The manuscript requires a section presenting examples of unimodal, bimodal, and trimodal distributions with criteria for classification. This addition would enable readers to understand the similarities between distributions such as the yellow and orange DSDs in Fig 7B.*

Answer: We thank the reviewer for this constructive comment. In the revised manuscript, we have added a new section A2 in the appendix to explicitly clarify (1) the algorithmic criteria used to identify the number of modes in each DSD and (2) the representative examples of unimodal, bimodal, and trimodal DSDs, together with an explanation of how they are classified into these categories. The classification criteria are described in both Appendix A2 and the *Data set and methods* section. For example, in the *Data set and methods* section:

"*For each DSD, unimodal, bimodal, and trimodal gamma and lognormal fits were performed, yielding the corresponding sets of fitting parameters as well as the individual modal components. A*

fit was retained only if adjacent modal components intersected (mode 1-2 for bimodal fits; mode 1-2 and mode 2-3 for trimodal fits). The turning diameter D_{turn} *was identified as the diameter of the first intersection of two adjacent modes, indicating that the mode begins at the next bin. If the first size bin of the DSD had the highest number concentration, it was identified as* D_{turn} *of the first mode. A fit was accepted only if all identified* D_{turn}*s did not fall within the same or adjacent size bins. Finally, the Akaike Information Criterion (AIC) and the Bayesian Information Criterion (BIC) are used to evaluate the performance of the accepted fits.*"

The six examples presented in Appendix A2, except for example of the unimodal DSD, other examples correspond to the DSDs mentioned in the reviewer's comments, for example:

"*Triple mode examples:*

Figure A7 shows the mode identification result for the yellow curve prior to the maximum LWC in F10 (Figure 8b). In the trimodal fit (d), intersections exist between mode 1 and mode 2 as well as between mode 2 and mode 3, and the resulting D_{turn} *satisfy the physical requirement that they do not fall within the same or adjacent bins. Moreover, this fit yields the minimum combined AIC and BIC among all fits. Therefore, it is used to define the number of modes and the* D_{turn} *of this DSD.*

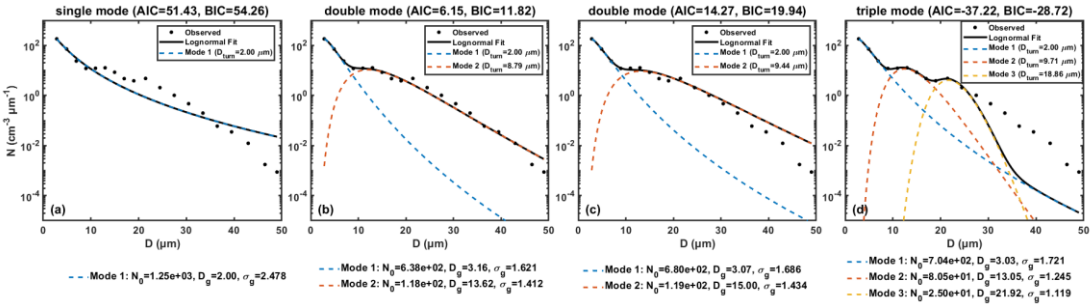

Figure A7 example of triple mode DSD."

In Appendix A6, we additionally discuss the sensitivity of segmented gamma and lognormal fits to the exclusion of potential peaks in the 30-50 μm range. For example:

"*To examine the impact of excluding potential modes in the 30-50 μm range on segmented gamma and lognormal fitting, an additional segmentation points at 40 μm was considered. Using the same approach as in Section 3.4, segmented fits were applied to all DSDs, and the fitting results were used to retrieve* N_f*, LWC,* R_v*,* R_{eff}*, absorption coefficient and optical thickness. The deviations of these retrieved quantities from the observations were then calculated. Figure A19 compares the deviations obtained from fits with segmentation points at 10 and 20 μm and those including the additional 40 μm segmentation point. The results show that introducing the 40 μm segmentation point does not lead to a significant improvement in fitting performance, indicating that the omission of potential modes larger than 30 μm does not substantially affect the results of this study.*"

Comments: *Furthermore, an analysis of multimodal DSD evolution is needed to reconcile the*

contradictions in the results. The manuscript must provide an answer: are triple-mode DSDs associated with broader or narrower size distributions? If the relationship is context-dependent, what mechanisms govern the observed variability?

Answer: Thank you for the suggestion. In the Conclusions, we summarize the relationship between different DSD mode types and the fog life cycle as well as key microphysical variables, discuss the possible physical mechanisms, and outline the limitations of the study along with perspectives for future work. For example:

About the relationship between different DSD mode types and the fog life cycle:

"*Among all fog cases, radiation fog accounts for the largest proportion and radiation-advection fog tends to persist longer. Variations in the number of DSD modes are closely linked to fog lifecycle characteristics and to changes in physical variables such as* N_f *and LWC. For fog events with relatively low* N_f *and LWC or relatively less intense formation and dissipation processes, transitions in DSD modal type are infrequent and occur mainly during the formation and dissipation stages. When* N_f *and LWC increase sharply, the DSD shows frequent modal transitions with an increasing prevalence of bimodal DSD. Moreover, when* N_f *and LWC exhibit strong oscillations, transitions among different modal types occur simultaneously and at high frequency.*"

About the outline the limitations of the study:

"*It should be noted that this study is primarily based on observational data and focuses on analyzing the microphysical characteristics and their evolutions. The underlying physical processes and mechanisms governing fog evolution as well as the interactions and relative importance of different controlling factors, remain to be clarified through enhanced analyses of aerosol background conditions and sensitivity experiments on relevant physical processes using numerical simulations. In addition, only a three-parameter gamma and lognormal distribution was used to fit and refine the mean DSD. The comparative performance of alternative distribution and evaluate the influence of different parameterizations on fitting accuracy could be explored in future studies.*"